Analysis of a High-Velocity Oxygen-Fuel (HVOF) Thermal Spray Torch
Part 1: Numerical Formulation

W.L. Oberkampf and M. Talpallikar

The fluid and particle dynamics of a high-velocity oxygen-fuel torch are analyzed using computational fluid dynamic techniques. The thermal spray device analyzed is similar to a Metco Diamond Jet torch with powder feed. The injection nozzle is axisymmetric with powder and a carrier gas injected on the centerline, premixed fuel and oxygen fed from an annulus, and air cooling injected from an annulus along the interior surface of the aircap. The aircap is a conically converging nozzle that achieves choked flow conditions at the exit; a supersonic, underexpanded jet develops externally. A two-dimensional, axisymmetric geometry is assumed; the equations for mass, momentum, and energy conservation are solved for both the gas and the particle phases. The combustion process is modeled using approximate equilibrium chemistry with dissociation of the gas with a total of nine species. Turbulent flow is modeled by a two-equation model for turbulent kinetic energy and dissipation rate that includes compressibility effects on turbulent dissipation. Particles are modeled as a lumped-heat-capacity system and are considered to melt upon attaining the required latent heat of fusion. An iterative, implicit, finite-volume numerical method is used to solve the coupled gas and particle equations inside and outside the torch. A companion paper presents the results of the numerical simulation and discusses in detail the gas and particle dynamics.

1. Introduction

1.1 Background

THERMAL spraying using the high-velocity oxygen-fuel (HVOF) process is used to apply metallic, ceramic, and composite coatings to a variety of substrates in order to improve wear resistance, abrasion resistance, thermal and electrical insulation, and corrosion protection. Coatings applied using HVOF spraying have high mass density and possess good bond and mechanical strength. Spray torches for HVOF use a combustion process to heat the flowing gas and the coating material and then to accelerate the gas/particle two-phase flow to high velocities. The gas and particle velocities are commonly much higher than those achieved using plasma spraying. The high particle velocities result from two factors. First, HVOF torches normally produce supersonic external flows, whereas plasma torches normally operate with a subsonic stream. Second, gas density in HVOF torches is typically much higher than in plasma torches because the peak gas temperatures in HVOF torches are much lower. The maximum gas temperature in HVOF spraying is typically 3000 K; in plasma spraying, roughly 10,000 K. The combination of high gas velocity and high gas density accelerates the spray particles to significantly higher speeds, thereby tending to produce higher-density coatings.

W.L. Oberkampf, Aerosciences and Compressible Fluid Dynamics Department, Sandia National Laboratories, Albuquerque, NM 87185-0825, USA; and **M. Talpallikar,** CFD Research Corporation, Huntsville, AL 35805, USA.

1.2 Previous Investigations

Two in-depth, experimental investigations have been undertaken to improve the physical understanding of the gas dynamics, turbulence, and particle characteristics of HVOF spraying. Kowalsky et al. (Ref 1) experimentally investigated Flame-Spray Industries' CDS torch. This torch uses propylene and oxygen for combustion and a powder feed for particle injection. Velocities of alumina, tungsten carbide, and tribaloy particles in the torch plume were measured using laser two-focus velocimetry. Pressure measurements inside the torch and photographic measurements were made to determine various gas dynamic characteristics of the torch. Hackett et al. (Ref 2) investigated the external gas dynamics of the Hobart-Tafa JP-5000, particularly the free-jet mixing of the high-temperature plume with the surrounding atmosphere. This torch uses a liquid kerosene fuel-injection system, which atomizes the fuel and reacts with gaseous oxygen.

The first quantitative analysis of the gas dynamics and particle dynamics of HVOF spraying was conducted by Thorpe and Richter (Ref 3). They analyzed the internal and external flow of a newly designed HP/HVOF torch from Hobart TAFA Technologies, which is similar to the Union Carbide D-Gun. They computed the energy release from an equilibrium chemistry model of heptane and oxygen, assuming no influence from the gas motion, and used one-dimensional isentropic flow assumptions to compute the flow through a converging/diverging section of the nozzle. One-dimensional flow assumptions were then used to compute the effect of friction (Fanno flow) in the constant-diameter barrel of the torch. External to the torch they used the linearized shock-expansion theory to calculate the underexpanded supersonic jet flow, ignoring mixing with the ambient air. Particle trajectories were also calculated, assuming no interaction with the gas stream.

Recent analyses have used modern computational fluid dynamic (CFD) methods to simulate more complex physics in two dimensions. Some improvements in thermal spray modeling resulted from computational techniques developed for gas turbine engines and liquid and solid rocket motors. Axisymmetric and planar two-dimensional CFD simulations of chemically reacting, dissociated and ionized flows, along with state-of-the-art turbulence models, have been presented in the literature. Researchers who have modeled thermal spray problems have used a Eulerian description of the gas flow and either a Eulerian or Lagrangian* description of the dispersed phase (i.e., the particles). The influence of the particulate phase, either liquid or solid particles, on the continuous phase is taken into account by including interphase coupling terms in the equations. Some analyses, however, have completely ignored the coupling of the particulate phase and the gas phase. These simulations compute the effect of the flow on the particles, but do not allow an effect of the particles on the flow. In the Eulerian-Eulerian approach, sometimes referred to as the two-fluid method, a description similar to that of the continuous phase is also used for the particulate phase. In the Eulerian-Lagrangian approach, a relatively small number of computational particles are used to model a large collection of physical particles, either solid or liquid. Each approach has its strengths and weaknesses, but it is generally believed that the Eulerian-Lagrangian approach is superior for modeling spray phenomena.

Ramshaw and Chang (Ref 4) modeled a thermal plasma using a two-dimensional CFD approach with extensive plasma physics. The plasma was modeled as a multicomponent, chemically reacting gas in local thermodynamic equilibrium. Ionization, dissociation, recombination, and other chemical reactions were computed by general kinetic equilibrium chemistry algorithms. No particulates were included in the simulation. Chang (Ref 5) used a similar computational approach to model alumina spraying in an argon-helium plasma jet. The plasma is represented as a continuous multicomponent, chemically reacting ideal gas with temperature-dependent thermodynamic and transport properties. These formulations, as most techniques, solve the numerical equations with a time-marching or iterative scheme until a steady-state solution is achieved. The time-marching technique, however, is an explicit scheme that requires very long computer run times when high spatial resolution is required.

Various investigators have used CFD techniques to model the spray forming, or spray casting, process. El-Haggar and Crowe (Ref 6) modeled the external two-phase flow, including the stagnation of the flow on a flat substrate. They used a PSI-Cell (particle-source-in-cell) method and a finite-difference method to solve the coupled two-phase flow equations. The velocities were small at the nozzle exit and the temperature was relatively low, so no compressibility or chemistry effects were considered. Berry et al. (Ref 7) modeled the gas flow and liquid metal stream atomization inside a spray forming nozzle. They considered liquid metal injection from a slot at the throat of a converging-diverging nozzle for planar two-dimensional flow.

They used a density-based formulation for the gas phase and an implicit, time-iterative, finite-difference method to solve the equations. As in the study by El-Haggar and Crowe, the gas temperature and flow velocities were low, so no chemistry effects were considered and the flow was essentially incompressible.

Power et al. (Ref 8) and Smith et al. (Ref 9) conducted the first CFD simulation of the HVOF spraying process. They modeled both the internal and external flow of the Metco Diamond Jet torch. In this torch, powder is fed through a center tube using nitrogen as a carrier gas. Premixed oxygen and propylene are injected through an annulus in the nozzle. This annulus is a simplification of the eight small holes located circumferentially around the nozzle to introduce premixed fuel and oxygen. Air is injected in an outer annulus between the nozzle and the aircap to cool the aircap, since the torch has no other cooling mechanism. The combusting subsonic flow was modeled inside the converging aircap, and the flow became choked at the exit of the aircap; that is, it attained the sonic condition. External to the torch, they modeled the decay of the supersonic jet in a quiescent atmosphere. Because the pressure in the torch was greater than atmospheric pressure at the exit, the jet was underexpanded. The flow then expanded exterior to the aircap and formed "shock diamonds" commonly seen in supersonic underexpanded streams. Their CFD simulation included a turbulence model for turbulent kinetic energy (k) and dissipation rate (ε) and combustion chemistry. Their chemistry model included dissociation of the reaction products using a two-step, finite-rate chemistry model and seven gas species: C_3H_6, O_2, N_2, H_2O, CO_2, CO, and H_2. The finite-difference equations, using a density-based formulation, were solved by an explicit time-iterative scheme. Tracker particles of various sizes that responded to local gas velocity and temperature were injected inside the aircap near the centerline, but did not interact in any way with the gas stream. The analysis also did not account for any phase change of the particles.

1.3 Present Investigation

This paper presents the formulation and numerical methods of a CFD analysis of an HVOF torch geometry similar to the Metco Diamond Jet torch. A companion paper (Ref 10) presents the results of the numerical simulation and discusses the gas dynamics and particle dynamics of HVOF thermal spraying. The analysis uses a Eulerian and Lagrangian formulation for the gas and particle phases, respectively. A k-ε turbulence model is used, which includes compressibility correction terms to account for the decrease in turbulent mixing that occurs for supersonic flow. Combustion is modeled by an approximate equilibrium chemistry model that accounts for dissociation of the combustion products. Dissociation strongly limits the rise in the gas temperature because much of the thermal energy released from combustion is consumed in breaking the chemical bonds of the product species. Solid particles are introduced near the centerline of the aircap and are strongly coupled to the numerical solution of the gas phase. Momentum and thermal energy are exchanged between the particulate and gas phases. Particles are modeled as a lumped-heat-capacity system and are considered to melt upon attaining the required latent heat of fusion at the melt temperature. Details of the mathematical and numerical modeling and

---

*In the Eulerian viewpoint, equations of motion are written for a fixed, but arbitrarily located, point in space. In the Lagrangian viewpoint, equations are written for a specific fluid element or particle.

solution technique are given, along with computer resources required to obtain the computational results.

2. Mathematical Modeling

The mathematical model of the gas flow and particle physics was composed of several elements: torch geometry, modeling of the gas phase, fluid dynamic turbulence, reacting flow chemistry, and solid/liquid particle dynamics. These modeling elements are distinct topics from numerical solution issues, that is, approximate mathematical representation of the continuum physics in terms of difference equations and the subsequent computer solution of these equations. Only a summary of the mathematical and numerical modeling will be given here. The present analysis uses the computer code CFD-ACE, which is commercially available from CFD Research Corporation (Huntsville, AL). For more information on the general mathematical formulation and numerical methods in CFD-ACE, see Ref 11 and 12.

2.1 Torch Geometry

The geometry chosen for the present analysis is similar to the Metco Diamond Jet torch. Figure 1 shows the internal geometry of the conceptual torch being analyzed. The present geometry captures all of the important gas dynamics and particle dynamics typical of this HVOF torch design. The conceptual torch is of an axisymmetric, two-dimensional geometry; that is, rotational symmetry is assumed. The central stream uses argon as the carrier gas to inject solid spherical particles of copper through a circular tube. The second stream injects premixed propylene and oxygen through an annulus at an angle of 5° to the centerline. In the Metco Diamond Jet torch, premixed propylene and oxygen are injected through eight small tubes circumferentially spaced equally around the nozzle. To keep the analysis tractable, a two-dimensional axisymmetric annulus for injection of premixed fuel and oxygen is assumed, whereas the actual hardware produces three-dimensional flow around each fuel/oxygen tube. The third stream injects air through an annulus at an angle of 5° adjacent to the wall for cooling of the aircap. The mass flow rate
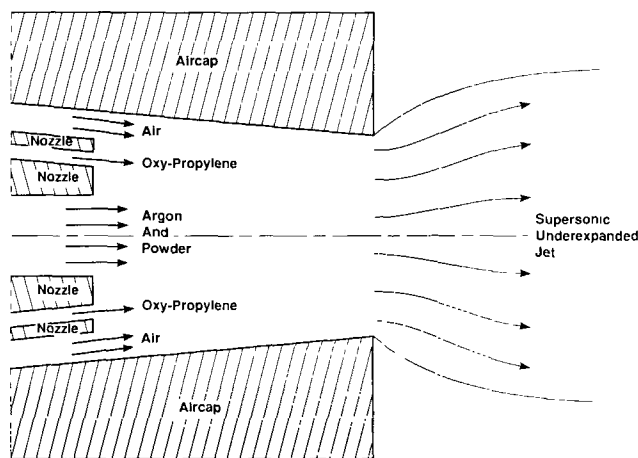

Fig. 1 Schematic of HVOF thermal spray torch

of each gas stream is specified, as well as the mass flow rate and size of the spherical particles in the central stream. The aircap geometry is a 5° half-angle, conically converging channel that attains a minimum area at a distance of 10 mm from the injection location. The torch is assumed to exhaust to ambient conditions consisting of air at room temperature and sea-level pressure. To simplify the external geometry, the aircap is assumed to have a large outside diameter; i.e., a solid wall extends radially at the exit of the aircap.

The general character of the internal flow field is a release of thermal energy from the oxypropylene combustion and a resulting increase in pressure inside the aircap. The premixed oxypropylene stream is assumed to begin combusting as soon as it enters the computational domain. The combustion can also include oxygen from the adjacent air stream. The pressure is sufficient in the aircap to choke the flow through the aircap exit; that is, Mach one is attained at the exit of the aircap. Because the pressure in the exit plane is greater than the ambient pressure condition, the aircap flow is said to be underexpanded. The flow will expand supersonically external to the aircap so as to meet the ambient pressure condition. The external pressure adjustment of the supersonic stream occurs through an alternating series of expansion and compression waves. Certain portions of the compression waves coalesce into shock waves. The luminescence of the flow after these shock waves is normally referred to as "shock diamonds." The perimeter of the supersonic stream immediately begins turbulent mixing with the ambient air and, consequently, the gas velocity decreases. After several shock diamonds, the flow decays to subsonic conditions while entraining increasing amounts of cool ambient air. The numerical simulation terminates at an axial distance of 20 aircap radii from the exit plane, a location where the flow is near sonic conditions.

2.2 Gas Phase Modeling

The governing equations for a dilute gas/particle mixture are the conservation of mass, momentum, and energy for unsteady, compressible, turbulent flow. The dilute assumption implies that the particulate phase occupies negligible volume fraction of the flow and that the particles are collisionless. Consequently, the coupling between the gas and particulate phases is modeled by source terms expressing the transfer of momentum and energy between the two phases. These equations are written in Cartesian tensor form:

$$\frac{\partial \bar{\rho}}{\partial t} + \frac{\partial (\bar{\rho}\,\tilde{u}_j)}{\partial x_j} = 0 \tag{Eq 1}$$

$$\frac{\partial (\bar{\rho}\tilde{u}_i)}{\partial t} + \frac{\partial (\bar{\rho}\,\tilde{u}_i\,\tilde{u}_j)}{\partial x_j} = \frac{\partial \bar{p}}{\partial x_i}$$

$$+ \frac{\partial}{\partial x_j}\left[(\mu + \mu_t)\left(\frac{\partial \tilde{u}_i}{\partial x_j} + \frac{\partial \tilde{u}_j}{\partial x_i} - \frac{2}{3}\frac{\partial \tilde{u}_m}{\partial x_m}\delta_{ij} \right) \right]$$

$$- \frac{2}{3}\frac{\partial (\bar{\rho}k)}{\partial x_i} + S_{M_i} \tag{Eq 2}$$

$$\frac{\partial(\bar{\rho}\tilde{H})}{\partial t} + \frac{\partial(\bar{\rho}\tilde{u}_j\tilde{H})}{\partial x_j} = -\frac{\partial}{\partial x_j}\left[(\Gamma + \Gamma_t)\frac{\partial\tilde{H}}{\partial x_j}\right]$$

$$+ \frac{\partial}{\partial x_j}\left[(\mu - \Gamma + \mu_t - \Gamma_t)\frac{\partial}{\partial x_j}\left(\frac{1}{2}\tilde{u}_k\tilde{u}_k\right)\right] + \frac{\partial\bar{p}}{\partial t}$$

$$+ \frac{\partial}{\partial x_j}\left[(\mu + \mu_t)\tilde{u}_i\left(\frac{\partial\tilde{u}_i}{\partial x_j} + \frac{\partial\tilde{u}_j}{\partial x_i} - \frac{2}{3}\frac{\partial\tilde{u}_k}{\partial x_k}\delta_{ij}\right)\right] + S_H \qquad \text{(Eq 3)}$$

where (–) denotes Reynolds averaged (i.e., time averaged) quantities and (~) denotes Favre averaged (i.e., density averaged) quantities; ρ is the fluid mass density; u_i is the ith Cartesian component of the velocity; p is the static pressure (that pressure experienced by a fluid element moving at the local gas velocity); μ is the molecular (laminar) viscosity of the gas; μ_t is the turbulent, or eddy, viscosity; δ_{ij} is the Kronecker delta; H is the total enthalpy of the gas and is defined by $H = h + (u_ju_j)/2$, where h is the static enthalpy; and Γ and Γ_t are the laminar and turbulent diffusivity coefficients, defined as μ/σ and μ_t/σ_t, respectively, where σ is the Prandtl number. The laminar viscosity and thermal conductivity are both functions of the local gas temperature. S_{M_i} and S_H are the momentum and total enthalpy source terms, respectively, for coupling the particle phase to the gas phase equations.

2.3 Turbulence Modeling

For turbulent flow, the Reynolds stress tensor is closed using the k-ε turbulence model of Launder and Spalding (Ref 13), where k is the turbulent kinetic energy and ε is the rate of dissipation of turbulent kinetic energy. These terms are computed throughout the flow field by solving the following partial differential equations:

$$\frac{\partial(\bar{\rho}k)}{\partial t} + \frac{\partial(\bar{\rho}\tilde{u}_jk)}{\partial x_j} = \bar{\rho}P - \bar{\rho}\varepsilon + \frac{\partial}{\partial x_j}\left[\frac{(\mu + \mu_t)}{\sigma_k}\frac{\partial k}{\partial x_j}\right] \qquad \text{(Eq 4)}$$

$$\frac{\partial(\bar{\rho}\varepsilon)}{\partial t} + \frac{\partial(\bar{\rho}\tilde{u}_j\varepsilon)}{\partial x_j} = C_{\varepsilon_1}\frac{\bar{\rho}P\varepsilon}{k} - C_{\varepsilon_2}\frac{\bar{\rho}\varepsilon^2}{k} + \frac{\partial}{\partial x_j}\left[\frac{(\mu + \mu_t)}{\sigma_\varepsilon}\frac{\partial\varepsilon}{\partial x_j}\right]$$

$$\text{(Eq 5)}$$

where P is the rate of production of turbulence and is given by:

$$P = \nu_t\left(\frac{\partial\tilde{u}_i}{\partial x_j} + \frac{\partial\tilde{u}_j}{\partial x_i} - \frac{2}{3}\frac{\partial\tilde{u}_m}{\partial x_m}\delta_{ij}\right)\frac{\partial\tilde{u}_i}{\partial x_j} - \frac{2}{3}k\frac{\partial\tilde{u}_m}{\partial x_m} \qquad \text{(Eq 6)}$$

The values of the empirical coefficients are

$$C_\mu = 0.09; C_{\varepsilon_1} = 1.44; C_{\varepsilon_2} = 1.92; \sigma_k = 1; \sigma_\varepsilon = 1.3$$

The turbulent viscosity, given by $\nu_t = (C_\mu k^2)/\varepsilon$, provides the coupling of the turbulence model to the Navier-Stokes, energy, and reacting flow equations. For high-speed flows, it is well known that the rate of turbulent dissipation decreases as the convective Mach number increases. If this effect is not included in the k-ε model, then high-speed turbulent jets are predicted to de-
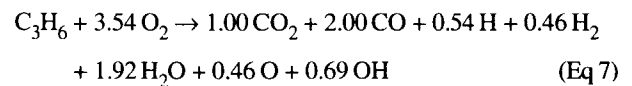
cay more rapidly than observed in experiments. The method of Sarkar (Ref 14) is used to modify the k-ε model for compressibility effects.

2.4 Chemical Reaction Modeling

Modeling of the chemical reactions also involves complex physics, similar to the modeling of turbulence. To make the chemistry modeling tractable, the chemical reaction rates are assumed to be much faster than the time scales associated with the gas dynamics. This assumption allows one to use equilibrium chemistry modeling. For the premixed stream of oxygen and propylene, this results in a reaction of the fuel and oxidizer as soon as the local temperature and pressure permit.

A full equilibrium chemistry model computes the gas species at each cell in the computational domain using the local temperature and pressure and minimizing the Gibbs free energy. This type of calculation is computationally intensive, and it strongly couples the flow solution to the chemistry modeling near the inlet of premixed streams. This approach was attempted for the present simulation, but numerical instabilities were encountered near the inlet of the premixed streams due to the strong coupling.

An approximate equilibrium chemistry model was used that yields the correct maximum temperature from an equilibrium chemistry computation and takes into account the dissociation of the gaseous products. If dissociation of the species is not included in the chemistry model, then the predicted temperatures will be unrealistically high, roughly by a factor of two for the present fuel and oxygen reactants. The approximate equilibrium chemistry model is referred to as the instantaneous chemistry model. In this model, the reaction is assumed to go to completion immediately upon entering the computational domain; in other words, regardless of the inflow temperature and pressure of the premixed gases, it is assumed that the reaction goes to completion at an infinitely fast rate. Given the specified oxygen/fuel mixture ratio (somewhat lower than the stoichiometric value of 4.5), the product species that result and their concentrations are determined from the one-dimensional equilibrium chemistry code developed by Gordon and McBride (Ref 15). The pressure and temperature specified for the one-dimensional equilibrium code approximate the inflow conditions of the premixed fuel and oxygen stream. It was found from this equilibrium calculation that at the specified initial temperature and pressure, unburned O_2 remained on the right side of the reaction equation. The excess oxygen was removed from the reaction equation and the result, written in moles, is

$$C_3H_6 + 3.54\,O_2 \rightarrow 1.00\,CO_2 + 2.00\,CO + 0.54\,H + 0.46\,H_2$$
$$+ 1.92\,H_2O + 0.46\,O + 0.69\,OH \qquad \text{(Eq 7)}$$

Flow mixtures in the computional domain are computed using mixture fractions. A mixture fraction of a given composition at any point in the flow field is defined as the mass fraction of that composition. Because the mixture fraction is a scalar that is transported by convection and diffusion, the following convection-diffusion equation governs the transport of mixture fraction:

$$\frac{\partial (\rho f_k)}{\partial t} + \frac{\partial (\rho u_j f_k)}{\partial x_j} = \frac{\partial}{\partial x_j}\left[(\Gamma + \Gamma_t)\frac{\partial f_k}{\partial x_j}\right] \qquad \text{(Eq 8)}$$

where f_k is the kth mixture fraction. For most turbulent flows at moderate to high Reynolds numbers, the effect of mass diffusivity among different species is negligible compared with convective transport.

2.5 Solid/Liquid Particle Modeling

The particle equations, for either solid or liquid particles, are solved in a Lagrangian frame of reference moving with the particles. The solutions to these equations are used to calculate the source terms for the momentum and energy gas phase equations. The equation of motion for the particle is written as (Ref 16):

$$m_p \frac{d\mathbf{V}_p}{dt} = \frac{1}{2}\rho A_p C_d (\mathbf{V} - \mathbf{V}_p)\,|\mathbf{V} - \mathbf{V}_p| - V_p \nabla p \qquad \text{(Eq 9)}$$

where m_p is the mass of the particle; $\mathbf{V}_p$ is the velocity vector of the particle; C_d is the drag coefficient of the particle; ρ, $\mathbf{V}$, and p are the density, velocity, and pressure of the gas, respectively; A_p is the droplet cross-sectional area; and V_p is the particle volume. All particles, solid or liquid, are assumed to be spherical. The equation of motion for a particle accounts for the acceleration/deceleration of the droplet due to the combined effects of drag from the gas flow and local pressure gradient in the gas.

The drag coefficient for the particle is based on the local Reynolds number of the particle and is evaluated as:

$$\text{Re} = \frac{\rho |\mathbf{V} - \mathbf{V}_p| d_p}{\mu} \qquad \text{(Eq 10)}$$

where d_p is the particle diameter and μ is the molecular viscosity of the gas. The following correlations have been found to be valid for a wide range of Reynolds numbers (Ref 16):

$$C_d = \begin{cases} \dfrac{24}{\text{Re}} & \text{for Re} < 1 \\[2mm] \dfrac{24}{\text{Re}}(1 + 0.15\,\text{Re}^{0.687}) & \text{for } 1 < \text{Re} < 10^3 \\[2mm] 0.44 & \text{for } > 10^3 \end{cases} \qquad \text{(Eq 11)}$$

The particles are modeled as a lumped-heat-capacity system; that is, the temperature is assumed uniform in the particle. The energy equation for the particle is written in two parts: one for particle temperature less than or greater than the melt temperature, and one for the particle at the melt temperature:

$$m_p (C_p)_p \frac{dT_p}{dt} = \pi d_p^2 \dot{q} \quad (\text{for } T_p \neq T_m) \qquad \text{(Eq 12a)}$$

$$m_p L_f \frac{d\chi_p}{dt} = \pi d_p^2 \dot{q} \quad (\text{for } T_p = T_m) \qquad \text{(Eq 12b)}$$

where $(C_p)_p$ is the specific heat of the particle, T_p is the particle temperature, $\dot{q}$ is the sensible heat flux to the particle, T_m is the melt temperature of the particle, L_f is the latent heat of fusion,

and χ_p is the fraction of the particle that has melted. The term $\dot{q}$ is calculated from:

$$\dot{q} = \frac{2\kappa\,(T - T_p)\,\text{Nu}}{d_p} \qquad \text{(Eq 13)}$$

where κ and T are the thermal conductivity and temperature of the gas, respectively. Nu is the Nusselt number and is obtained from the following correlation:

$$\text{Nu} = 2 + 0.6\text{Re}^{0.5}\sigma^{0.333} \qquad \text{(Eq 14)}$$

where σ is the Prandtl number of the gas phase.

3. Numerical Solution Technique

3.1 Finite-Volume Approximations

The discretization of the above differential equations is carried out using a finite-volume approach in two spatial dimensions, x and r. First, the solution domain is divided into a large number of discrete volumes or "cells," where all dependent flow variables and space transformation variables are stored at their geometric centers. The finite-volume approach is used because of its attractive capability of conserving flow quantities locally and globally. A collocated (i.e., nonstaggered) grid technique is used. The average value of any flow quantity within a control volume is given by its value at each cell center. The finite-volume numerical method for the gas dynamics uses the following dependent variables: pressure, two velocity components, total enthalpy, turbulent kinetic energy, rate of dissipation of turbulent kinetic energy, and mixture fraction for each gas species. The solution essentially involves integrating the gas dynamic, the turbulence model, and the mixture fraction equations over each control volume, with the particle effects coupled to the gas dynamic momentum and energy equations through source terms.

The finite-volume forms of the gas phase equations and the particle trajectory equations are transformed from physical space to computational space. This is done to greatly simplify the mesh on which the finite-difference equations are solved in computational space. In physical space, the mesh is fitted onto every surface so that a transformed coordinate matches each surface. That is, a surface-fitted grid in physical space is mapped onto a square (for two-dimensional problems) or a cube (for three-dimensional problems) in computational space. This is done using an independent variable transformation of the axisymmetric coordinates (x, r) to nonorthogonal coordinates (ξ, η) in computational space. A separate elliptic partial differential equation is solved, which transforms the physical space into computational space. The Jacobian of the transformation is then used to transform the gas phase and particle trajectory equations into computational space. In computational space, these equations are solved on a square domain with a uniformly spaced grid. The body-fitted-coordinate transformation technique is well known in the literature (see, for example, Ref 17).

The general form of the algebraic (discrete) equations for conservation of a dependent variable ϕ in a finite-volume p is given by:

$$A_p\phi_p = \sum_{nb} A_{nb}\phi_{nb} + S \qquad (\text{Eq } 15)$$

The coefficients A_{nb} contain both convective and diffusive fluxes, nb refers to all the neighbors of cell p in a general body-fitted coordinate system, and S is the source term. For two-dimensional problems, the differencing stencil involves nine cells. Because the independent variables are available only at the cell centers, the cell-face values need to be interpolated. For the diffusion terms, the value at the cell faces is determined by averaging the two adjacent cells. This results in a second-order-accurate central difference scheme. For the convection terms, the computer code has several options. A fully second-order upwind scheme was used for the convection terms in the continuity and momentum equations. A first-order upwind scheme was used for the convection terms in the energy, turbulence, and mixture fraction equations.

The continuity equation needs special treatment to resolve the velocity/pressure coupling to overcome the well-known checkerboard instability problem. Because the fluid density and velocities are available only at cell centers, cell-faced values need to be determined from cell-centered values. Linear interpolation between cell centers decouples the velocity and pressure fields, giving rise to the checkerboard instability. This instability is eliminated by using a procedure suggested by Rhie and Chow (Ref 18). In this method, the cell-face mass flux is evaluated by averaging the momentum equation to the cell faces and relating the cell-face velocity directly to the local pressure gradient. As a result, a fourth-order pressure damping term appears in the discrete form of the continuity equation.

3.2 Boundary Conditions and Grid Geometry

Figure 2 shows the computational domain for both the internal and external flow of the HVOF torch, along with the boundary conditions. The aircap generates a conically converging flow, with a 5° half-angle and an exit radius of 3.625 mm. The distance from the face of the nozzle, where all of the gases and powder are injected, to the exit plane of the aircap is 10 mm. The nozzle injects solid-phase, spherical copper particles with a diameter of 30 μm using argon as a carrier gas through a circular

tube with a radius of 1.5 mm. Premixed propylene (propene) and oxygen are injected through an annulus with a width of 0.5 mm and an inner radius of 2.5 mm. Air is injected through an annulus with a width of 1.0 mm and an inner radius of 3.5 mm. Both the oxyfuel and air are injected at an angle of 5° to the centerline of the torch (i.e., parallel to the surface of the aircap). All solid walls are assumed to be at a fixed temperature of 60 °C.

The mass flow rate of each injectant is given as follows:

$$\dot{m}_{argon} = 5.613 \times 10^{-4} \text{ kg/s} = 42.4 \text{ std ft}^3/\text{h}$$
$$\dot{m}_{copper} = 5.0 \times 10^{-4} \text{ kg/s} = 30 \text{ g/min}$$
$$\dot{m}_{propylene} = 1.116 \times 10^{-3} \text{ kg/s} = 80 \text{ std ft}^3/\text{h}$$
$$\dot{m}_{oxygen} = 3.561 \times 10^{-3} \text{ kg/s} = 340 \text{ std ft}^3/\text{h}$$
$$\dot{m}_{air} = 11.39 \times 10^{-3} \text{ kg/s} = 1200 \text{ std ft}^3/\text{h}$$

As can be seen from these flow rates, the fuel-to-oxygen mixture ratio is 3.19. This is less than the stoichiometric ratio of 4.5, as mentioned earlier. Also, note from the mass flow rate data that the mass loading of the copper particles to the total gas flow is 3%. For low mass loading such as this, one can ignore volumetric effects of the dispersed phase on the gaseous phase. All injectants are assumed to be at a temperature of 40 °C, and the gas flows are assumed to be turbulent.

The HVOF torch is assumed to exhaust into air (Fig. 2b) at a temperature of 30 °C and a pressure of 101 kPa (14.7 psia). The ambient air is assumed to be quiescent, except for the flow induced by the supersonic exhaust of the torch. As a result, air is entrained through the upper boundary of the computational domain and part of the downstream boundary. The velocity distribution of the air pumped in along the top boundary of the computational domain is determined by the numerical solution. The outflow boundary of the computational domain is defined to be 20 aircap exit radii from the exit plane of the torch. At the outflow boundary, a combined fixed pressure and extrapolated flow condition is used. If the boundary velocity is subsonic, then the fixed pressure condition is applied; if it is supersonic, then the extrapolation condition is applied.

Since an axisymmetric flow has been assumed, the computational grid need only encompass one-half of the physical domain of the torch—from the axis of symmetry to the outer radial boundary. The computational grid inside the aircap is composed of 70 axial cells and 48 radial cells (Fig. 3a). The computational
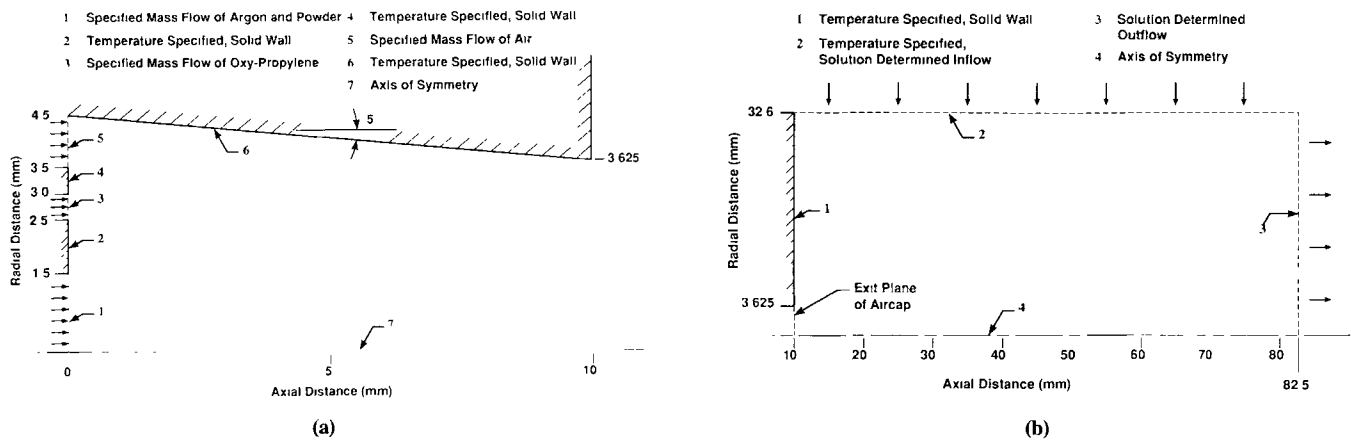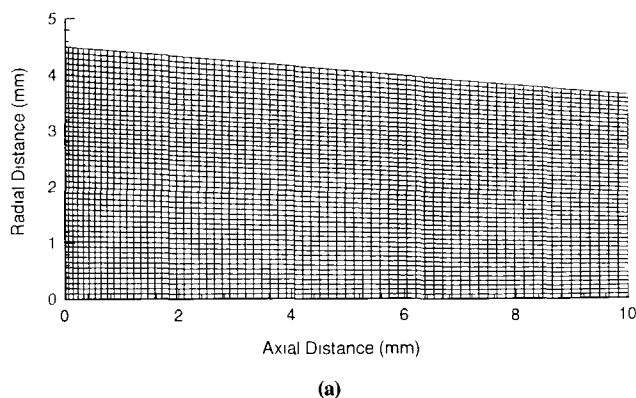

Fig. 2 Computational domain and boundary conditions (a) Inside the aircap (b) Outside the aircap

grid outside the aircap is composed of 80 axial cells and 100 radial cells (Fig. 3b). The total number of grid cells for the solution is 11,360. Inside the torch, the grid is uniformly spaced in the radial direction and is clustered in the axial direction. The ratio of the cell length (0.15 mm) at the exit plane of the aircap to a cell length (0.05 mm) at the nozzle face is 3. Outside the torch, the grid is highly clustered in both the radial and axial directions. The ratio of the cell height (1.0 mm) at the upper inflow boundary to the cell height (0.07 mm) on the centerline is 14. The ratio of the cell length (1.5 mm) at the right outflow boundary to the cell length (0.15 mm) at the exit plane of the aircap is 10.

3.3 *Iterative Solution Procedure*

The computer code CFD-ACE uses an iterative, segregated solution method, wherein the equation sets for each variable are solved sequentially and repeatedly until a converged solution is obtained. The overall solution procedure used is an extension of the SIMPLEC method. SIMPLEC, which stands for "semi-implicit method for pressure-linked equations consistent," was first proposed by Van Doormaal and Raithby (Ref 19). The overall solution procedure for the SIMPLEC algorithm is shown in Fig. 4. Two iteration parameters are specified by the user: N_ITER is the number of global iterations needed for convergence of the coupled gas/particle equations; C_ITER is the number of continuity and pressure correction iterations needed for numerical stability. The outer loop, the N_ITER loop, couples the energy, mixture fraction, and turbulence equations. This two-tiered level of coupling yields the highest rate of convergence, that is, the minimum computer time for a specified level of global convergence. Typical values for the present simulation were N_ITER = 3000 and C_ITER = 5.

The "solve" blocks shown in Fig. 4 involve the solution of large systems of simultaneous linear equations. These systems are referred to as "sparse" linear systems because the coefficient matrix has nonzero elements primarily near the main diagonal of the matrix. Iterative equation solvers are preferred for the solution because they are more economical in terms of memory requirements than direct solvers. The linear equation solver used for the present simulation is a type of "whole field" solver that is a modified version of the strongly implicit procedure (SIP) of Stone (Ref 20).

3.4 *Initial Conditions and Iterative Convergence*

The initial conditions are the values of all dependent variables in each cell in the computational domain for the first step of the iterative procedure. Although the values chosen are unimportant with respect to the final converged solution, they are important with regard to the speed with which the solution converges. For the first solution obtained, uniform flow with a constant temperature throughout was assumed. After various preliminary solutions were obtained, these converged solutions were used for initial solutions for more refined later solutions.

Iterative convergence is determined by the decrease in the magnitude of the sum of the squares of the residuals of each equation over the entire computational domain. The residual at a cell for a given finite-volume equation is defined as the difference between the left side of the equation and the right side of the equation at that cell; in other words, the residual is the magnitude of the imbalance of the finite-volume equation at a given cell. All solutions presented here have a minimum of five orders of magnitude decrease (from the initial peak value) in the *sum* of the magnitude of the residuals over the entire grid for each of the equations: continuity equation, u and v momentum equations, energy equation, k and ε turbulent kinetic energy equations, and the mixture fraction equation. Figure 5 shows a typical convergence history for the present simulation. The number of global iterations required for solution convergence varied from 2000 to 4000, depending on the accuracy of the initial conditions. It is generally accepted that four or five orders of magnitude of decrease in the residuals of each of the equations is adequate for convergence of the solution (Ref 21).

3.5 *Computer Resources Required*

All solutions were computed using the UNIX operating system on scientific workstations. Solutions on a Sun Microsystems Sparc 10 (model 30) required 10 to 15 h when the copper particles were not included (i.e., when only the gas phase was computed). When the copper powder injection was added to the simulation and coupled to the gas phase, the solutions required 20 to 30 h of total CPU time, depending on the accuracy of the initial conditions. Little effort was made to minimize the computer time by choosing optimum relaxation factors as the solution converged. The computer memory required for solutions
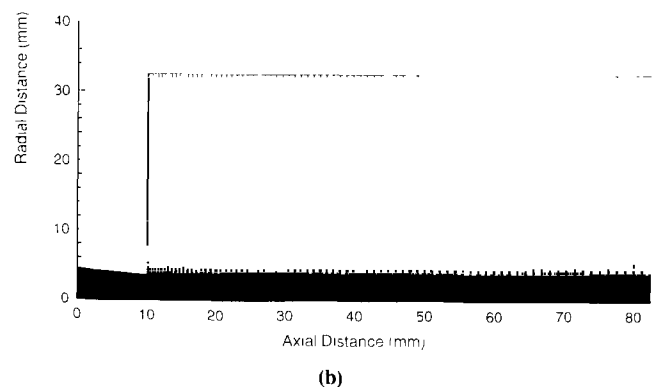
(a)

(b)

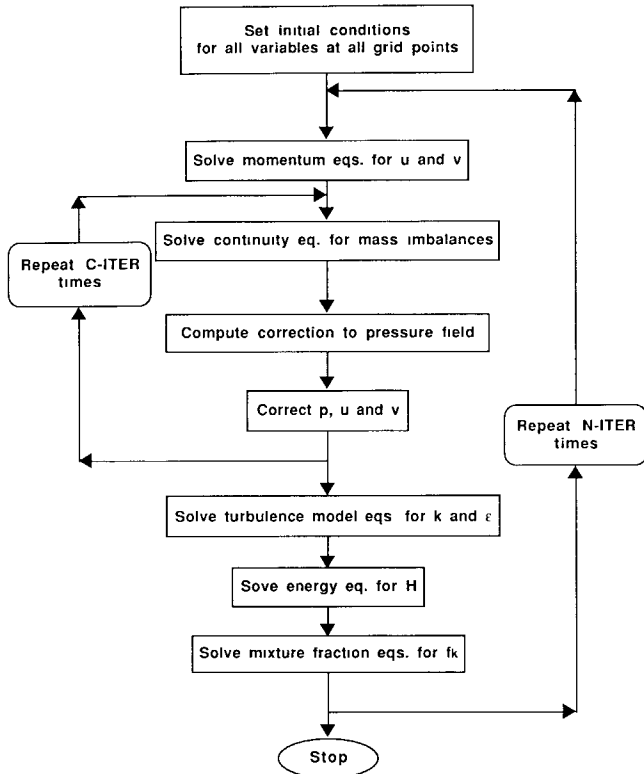**Fig. 3** Computational grids (a) Inside the aircap (b) Outside the aircap

Fig. 4 Iterative convergence procedure

Fig. 5 Convergence history of iterative solution (for data conditions given in section 3.3)

was roughly 20 MB. If this amount of memory is not available in RAM, convergence time significantly increases because the CPU is idle while the RAM memory is swapped back and forth to disk storage.

4. Summary and Conclusions

The mathematical formulation and numerical methods of a computational fluid dynamic analysis for a geometry similar to the Metco Diamond Jet torch have been presented. Modern CFD techniques provide a detailed mathematical simulation of the complex physical processes occurring in thermal spraying to guide improvements and optimization of the process. The analysis uses a Eulerian and Lagrangian approach for the gas and particles phases, respectively. A two-dimensional, axisymmetric geometry is assumed for the equations of mass, momentum, and energy conservation of both the gas and particle phases. Momentum and thermal energy are exchanged between the particulate phase and the gas phase. A k-ε turbulence model is used, which includes compressibility correction terms to account for the decrease in turbulent mixing that occurs for supersonic Mach numbers. Combustion is modeled by an approximate equilibrium chemistry model that accounts for dissociation of the combustion products. The iterative solution procedure to solve the finite-volume equations is discussed, along with the boundary conditions and structured grid geometry. For the 11,360 cells in the grid, roughly 25 h are required for a solution on a computer workstation. Computational results and discussion are given in a companion paper (Ref 10).
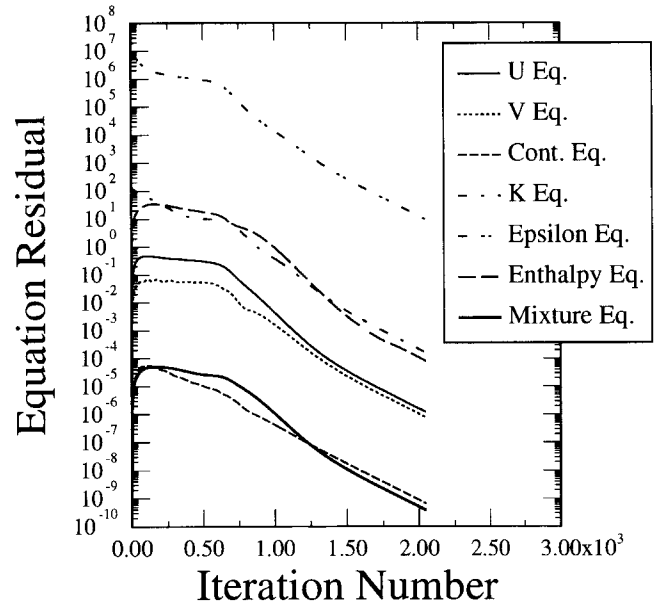
Nomenclature	
A_p	particle cross-sectional area
C_d	particle drag coefficient
C_p	specific heat
d_p	particle diameter
f_k	mixture fraction for the kth specie
H	total enthalpy per unit mass
k	turbulent kinetic energy
L_f	latent heat of fusion of the particle
m_p	particle mass
$\dot{m}$	mass flow rate of injectant
Nu	Nusselt number
P	rate of production of turbulent kinetic energy
p	pressure
$\dot{q}$	heat flux to the particle from the gas
Re	Reynolds number
S_H	total enthalpy source term due to particle phase
S_{M_i}	momentum source term due to particle phase
T	temperature
T_m	melt temperature of the particle
t	time
u_i	Cartesian velocity component in the ith direction
V_p	particle volume
V	velocity vector
x_i	Cartesian coordinate in the ith direction
Γ	laminar diffusion coefficient, μ/σ
Γ_t	turbulent diffusion coefficient, μ_t/σ_t
δ_{ij}	Kronecker delta
ε	rate of turbulence dissipation
κ	thermal conductivity
μ	molecular (laminar) viscosity
ρ	mass density
σ	Prandtl number of the gas phase

References

1. K.A. Kowalsky, D R. Marantz, M.F Smith, and W L. Oberkampf, HVOF Particle, Flame Diagnostics and Coating Characteristics, *Thermal Spray Research and Applications*, T.F. Bernecki, Ed , ASM International, 1991, p 587-592

2. C.M. Hackett, G S Settles, and J.D Miller, On the Gas Dynamics of HVOF Thermal Sprays, *Thermal Spray Coatings. Research, Design and Applications*, C.C Berndt and T.F. Bernecki, Ed., ASM International, 1993, p 167-172

3 M.L Thorpe and H.H. Richter, A Pragmatic Analysis and Comparison of the HVOF Process, *Thermal Spray: International Advances in Coatings Technology*, C C. Berndt, Ed., ASM International, 1992, p 137-147

4 J.D. Ramshaw and C.H. Chang, Computational Fluid Dynamics Modeling of Multicomponent Thermal Plasmas, *Plasma Chem. Plasma Process.*, Vol 12 (No. 3), 1992, p 299-325

5 C.H. Chang, Numerical Simulation of Alumina Spraying in an Argon-Helium Plasma Jet, *Thermal Spray: International Advances in Coatings Technology*, C C Berndt, Ed., ASM International, 1992, p 793-798

6. S.M El-Haggar and C.T. Crowe, "A Two-Dimensional Spray Model for the Spray-Casting Process," Paper No. 93-FE-4, presented at ASME Fluids Engineering Conf. (Washington, DC), June 1993

7. R A. Berry, H J. Gibeling, and F.J de Jong, "Multidimensional Calculation of Two-Phase Flow in a Spray-Forming Nozzle Using Eulerian-Lagrangian Analysis," Paper No. 93-FE-1, presented at ASME Fluids Engineering Conf. (Washington, DC), June 1993

8. G D. Power, T.J. Barber, and L.M Chiappetta, "Analysis of a High-Velocity Oxygen-Fuel (HVOF) Thermal Torch," AIAA Paper No 92-3598, presented at AIAA/SAE/ASME/ASEE 28th Joint Propulsion Conf. (Nashville, TN), July 1993

9. E.B Smith, G.D. Power, T J Barber, and L M. Chiappetta, Application of Computational Fluid Dynamics to the HVOF Thermal Spray Gun, *Thermal Spray: International Advances in Coatings Technology*, C C. Berndt, Ed., ASM International, 1992, p 805-810

10. W L. Oberkampf and M. Talpallikar, Analysis of a High-Velocity Oxygen-Fuel (HVOF) Thermal Torch, Part 2. Computational Results, *J. Therm. Spray Technol.*, Vol 5 (No 1), 1996

11 Y.G. Lai, A.J. Przekwas, and R.M C So, "Aerodynamic Flow Simulation Using a Pressure-Based Method and a Two-Equation Turbulence Model," AIAA Paper No. 93-2902, presented at AIAA 24th Fluid Dynamics Conf (Orlando, FL), July 1993

12 Y. Jiang, Y.G. Lai, S.Y. Ho, and A.J Przekwas, "3D Simulations of Complex Flows with an Implicit Multi-Domain Approach," AIAA Paper No. 93-3124, presented at AIAA 24th Fluid Dynamics Conf. (Orlando, FL), July 1993

13. B.E Launder and D.B Spalding, The Numerical Calculation of Turbulent Flows, *Comput. Meth. Appl. Mech. Eng.*, Vol 3, 1974, p 269-289

14. S Sarkar, The Analysis and Modeling of Dilatational Terms in Compressible Turbulence, *J. Fluid Mech.*, Vol 227, 1991, p 473-493

15. S Gordon and B.J. McBride, "Computer Program for Calculation of Complex Chemical Equilibrium Compositions, Rocket Performance, Incident and Reflected Shocks, and Chapman-Jouquet Detonations," NASA SP-273, 1976, new version, 1989

16. C T Crowe, M P Sharma, and D.E Stock, The Particle-Source-in-Cell (PSI-CELL) Model for Gas-Droplet Flows, *J. Fluids Eng.*, Vol 99 (Ser 1, No 2), 1977, p 325-332

17. *Numerical Grid Generation*, J F. Thompson, Ed , Elsevier Science, 1982

18. C M Rhie and W L Chow, Numerical Study of the Turbulent Flow Past an Airfoil with Trailing Edge Separation, *AIAA, J.*, Vol 21 (No. 11), 1983, p 1525-1532

19 J.P. Van Doormaal and G D. Raithby, Enhancements of the SIMPLE Method for Predicting Incompressible Fluid Flows, *Numer. Heat Transfer*, Vol 7 (No. 2), 1984, p 147-163

20. H L Stone, Iterative Solution of Implicit Approximates of Multi-Dimensional Partial Differential Equations, *SIAM J. Numer. Anal.*, Vol 5 (No 3), 1968, p 530-558

21. W Shyy, *Computational Modeling of Fluid Flow and Interfacial Transport*, Elsevier, 1994, p 184-202